Angewandte International Edition Chemie

VIP **Xenon Fluorides** *Very Important Paper*

International Edition: DOI: 10.1002/anie.201507635
German Edition: DOI: 10.1002/ange.201507635

Syntheses and Structures of $F_6XeNCCH_3$ and $F_6Xe(NCCH_3)_2$

*Kazuhiko Matsumoto, Jamie Haner, Hélène P. A. Mercier, and Gary J. Schrobilgen**

In memory of Henry Selig

Abstract: *Acetonitrile and the potent oxidative fluorinating agent XeF_6 react at −40°C in Freon-114 to form the highly energetic, shock-sensitive compounds $F_6XeNCCH_3$ (**1**) and $F_6Xe(NCCH_3)_2{\cdot}CH_3CN$ (**2**·CH_3CN). Their low-temperature single-crystal X-ray structures show that the adducted XeF_6 molecules of these compounds are the most isolated XeF_6 moieties thus far encountered in the solid state and also provide the first examples of Xe^{VI}–N bonds. The geometry of the XeF_6 moiety in **1** is nearly identical to the calculated distorted octahedral (C_{3v}) geometry of gas-phase XeF_6. The C_{2v} geometry of the XeF_6 moiety in **2** resembles the transition state proposed to account for the fluxionality of gas-phase XeF_6. The energy-minimized gas-phase geometries and vibrational frequencies were calculated for **1** and **2**, and their respective binding energies with CH_3CN were determined. The Raman spectra of **1** and **2**·CH_3CN were assigned by comparison with their calculated vibrational frequencies and intensities.*

The stereochemical activity of the valence electron lone pair (VELP) of XeF_6 has been a subject of considerable interest for over 50 years. The three possible gas-phase geometries of XeF_6 are an octahedral structure (**3**), where the Xe VELP is stereochemically inactive, a monocapped octahedral (C_{3v}) structure (**4**), and the C_{2v} structure (**5**). Gaseous XeF_6 has been studied by electron diffraction,[1–5] far-infrared,[6] Raman,[7,8] and photoelectron[9,10] spectroscopy. It has been concluded that the gas-phase structure of monomeric XeF_6 has C_{3v} symmetry (**4**), as predicted by the VSEPR model[11] for an AX_6E molecule and by previous quantum-chemical calculations.[12]

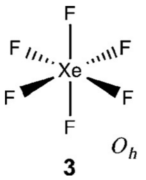

3

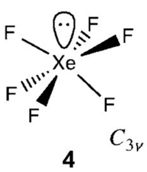

4

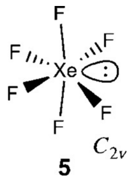

5

Explicitly correlated CCSD(T)-F12b calculations indicate that the lowest energy conformer of gaseous XeF_6 is **4** and the highest energy conformer is **3**.[12] Calculations with the spin-free exact two-component theory in its one-electron variant (SFX2C-1e) indicate that both **3** and **4** are minima[13] on the potential energy surface. Structure **5** is a transition state at both levels of theory. Although XeF_6 has been extensively studied by single-crystal X-ray diffraction, none of its seven known crystal modifications[14] contain XeF_6 (C_{3v}) molecules that are well-isolated from one another. Five phases contain ionic oligomers, $(XeF_5{}^+F^-)_n$ ($n = 4$ or 6), and two of the modifications, formulated as $(XeF_5{}^+F^-)_3{\cdot}XeF_6$, contain coordinated XeF_6 molecules with local symmetries that are close to C_{2v}. Similarly, the $[Xe_2F_{13}]^-$ anion in its $[NO_2]^+$ salt may be formulated as a $[XeF_7]^-$ anion that is fluorine-bridged to an XeF_6 (C_{2v}) molecule.[15] Low-temperature solution ^{19}F and ^{129}Xe NMR spectroscopy has shown that XeF_6 exists as a fluxional $(XeF_6)_4$ tetramer in which the four Xe and 24 F atoms are chemically equivalent on the ^{19}F and ^{129}Xe NMR time scales and the ^{129}Xe–^{19}F couplings are averaged.[16,17] The gas-phase ^{19}F and ^{129}Xe NMR spectra of XeF_6 display broad singlets.[18] Prior to this work, no examples of Xe^{VI}–N bonds had been reported. A considerable number of Xe^{II}–N species in which Xe is bonded to sp-, sp^2-, or sp^3-hybridized N atoms are known,[19] whereas only three examples of Xe^{IV}–N bonds have been reported, $[C_6F_5XeF_2][BF_4]{\cdot}(NCCH_3)_n$ ($n = 1$ or 2)[20] and $F_2OXeNCCH_3$.[21]

A 1:1 complex between XeF_6 and CH_3CN was formed by their stoichiometric reaction in Freon-114 (1,2-dichlorotetrafluoroethane) at −40°C [Eq. (1)]. The resulting adduct was soluble, giving a colorless solution. Removal of Freon-114 at −78°C resulted in a white powder, which rapidly decreased in volume under dynamic vacuum at −78°C, suggesting that **1** had formed a weak Freon-114 solvate. A 1:3 complex of XeF_6 and CH_3CN was prepared in a similar manner using a 1:3 ratio of XeF_6 and CH_3CN [Eq. (2)]; however, there was no evidence for the formation of a Freon-114 solvate.

$$XeF_6 + CH_3CN \xrightarrow[-40\,^{\circ}C]{\text{Freon-114}} F_6XeNCCH_3 \qquad (1)$$

$$XeF_6 + 3\,CH_3CN \xrightarrow[-40\,^{\circ}C]{\text{Freon-114}} F_6Xe(NCCH_3)_2 \cdot CH_3CN \qquad (2)$$

Solid samples of **1** and **2**·CH_3CN proved to be kinetically stable at −78°C, but detonated when mechanically shocked at this temperature. Both compounds slowly lost CH_3CN under dynamic vacuum at −40 to −20°C. Attempts to prepare **2** using a 1:2 molar ratio of XeF_6/CH_3CN yielded a mixture of **1** and **2**·CH_3CN. The addition of one equivalent of CH_3CN to **2**·CH_3CN led to a mixture of CH_3CN and **2**·CH_3CN with no evidence for $F_6Xe(NCCH_3)_3$ formation.

---

[*] Dr. K. Matsumoto, M. Sc. J. Haner, Dr. H. P. A. Mercier, Prof. G. J. Schrobilgen
Department of Chemistry, McMaster University
Hamilton, ON, L8S 4M1 (Canada)
E-mail: schrobil@mcmaster.ca

Supporting information and ORCID(s) from the author(s) for this article are available on the WWW under http://dx.doi.org/10.1002/anie.201507635.

Little information on the solution structure of **1** could be garnered from its ^{19}F and ^{129}Xe NMR spectra in SO_2ClF (see the Supporting Information for a full discussion).

Single crystals of **1** and **2**·CH_3CN suitable for X-ray crystal-structure determination were grown by slowly cooling their respective SO_2ClF and CH_3CN/Freon-114 solutions. The crystal structures of the isolated adducts and their calculated structures are in excellent agreement (Figure 1 and Figure 2, Tables S1 and S2; see the Supporting Information for a full discussion of the calculated geometries).

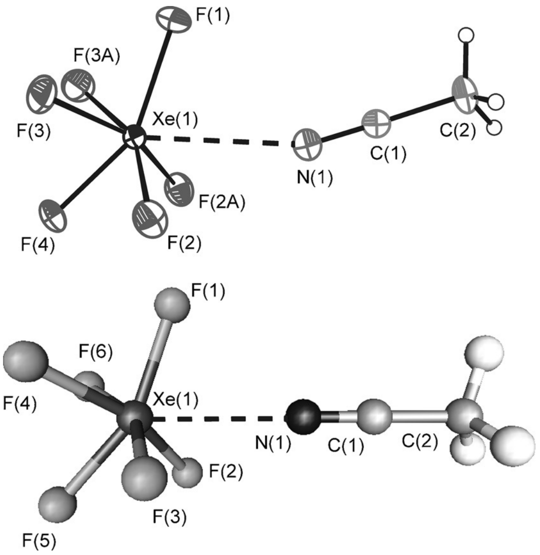

Figure 1. X-ray crystal structure of $F_6XeNCCH_3$ (top). Ellipsoids are shown at the 50% probability level. The calculated geometry (PBE1PBE/aug-cc-pVTZ(-PP)) for $F_6XeNCCH_3$ (bottom) is also shown.

The local symmetry of the XeF_6 moiety in **1** is approximately C_{3v} (Figure S1), whereas its crystal site symmetry is C_s. The Xe–N distance (2.762(2) Å) is significantly longer than the Xe^{II}–N distances in $[C_6F_5XeNCCH_3]^+$ (2.640(6)–2.610(11) Å),[22] but similar to the Xe^{IV}–N bond lengths in $F_2OXeNCCH_3$ (2.808(5), 2.752(5) Å)[21] and $[C_6F_5XeF_2][BF_4]$·$NCCH_3$ (2.742(4) Å).[20] The bond lengths are significantly shorter than the sum of the Xe and N van der Waals radii (3.71 Å),[23] but notably longer than Xe^{II}–N bonds (2.02(1)–2.236(4) Å).[19] The N1 atom of **1** is located on a pseudo-C_3 axis. The non-linear Xe1-N1-C1 angle (160.31(17)°) is likely the result of crystal packing and the deformability of this angle. The F atoms of the XeF_6 moiety comprise two groups, where F1, F2, and F2A form the most open trigonal face proximate to N1 and opposite to the most closed face, F3, F3A, and F4. The Xe VELP presumably resides between the Xe–F1, Xe–F2, and Xe–F2 bonds of the more open face. Correspondingly, the F-Xe-F angles [F1-Xe1-F2 and F1-Xe1-F2A: 115.65(4)°; F2-Xe1-F2A: 105.92(6)°] proximate to N1 are considerably more open than those of the opposite triad [F3-Xe1-F4 and F3A-Xe1-F4: 79.93(4)°; F3-Xe1-F3A: 82.59(8)°]. The difference between the average F-Xe-F angles of the open and closed faces is 29.53(6)°. The Xe–F bonds of the open face are significantly longer [Xe1–F1: 1.9769(13) Å; Xe1–F2/F2A: 1.9451(8) Å] than those of the closed face [Xe–F3/F3A: 1.8560(9) Å; Xe–F4: 1.8601(12) Å)]. At this time, it is not clear whether the C_{3v} geometry of **1** is imposed by CH_3CN or the presence of a sterically active Xe VELP. In the latter scenario, the Xe and N VELPs would oppose one another. Calculations are currently underway to ascertain the location of the Xe VELP. The average Xe–F bond length of **1** (1.907(2) Å) is comparable to those of other neutral Xe^{VI} species [$XeOF_4$: 1.890(2) Å;[24] XeO_2F_2: 1.899(3) Å[25]].

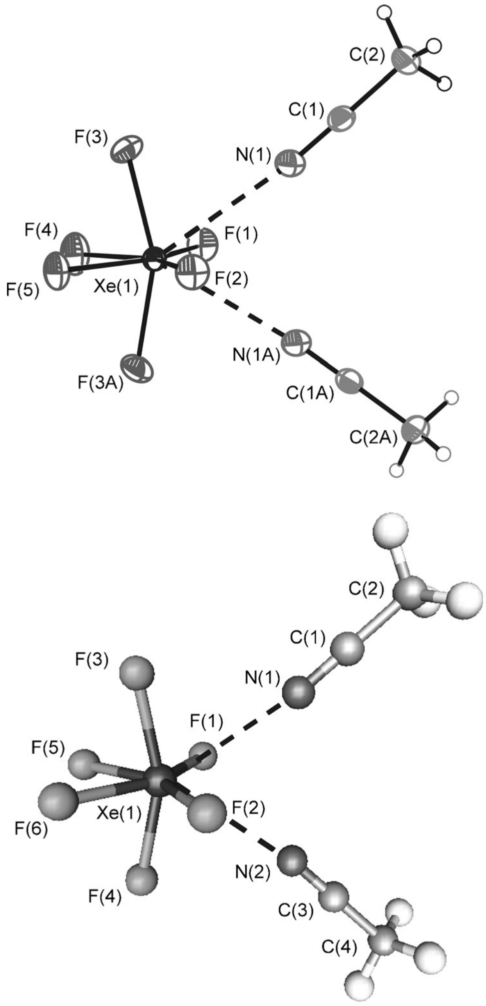

Figure 2. X-ray crystal structure of $F_6Xe(NCCH_3)_2$·CH_3CN. The lattice CH_3CN molecule is not shown (top). Ellipsoids are shown at the 50% probability level. The calculated geometry (PBE1PBE/aug-cc-pVTZ(-PP)) for $F_6Xe(NCCH_3)_2$ (bottom) is also shown.

Compound **2**·CH_3CN contains lattice CH_3CN molecules that lie in channels along the *b* axis and are twofold disordered along the *a* axis with a 50:50 population ratio (Figure S2). The crystal site symmetry of the XeF_6 unit is C_s; however, the isolated unit closely approximates C_{2v} symmetry. The Xe–N bond lengths (2.785(2) Å) of **2** are very similar to that of **1**. The N and C atoms of both coordinated CH_3CN molecules are approximately located on the pseudo-mirror plane bisecting the F1-Xe1-F2 and F4-Xe1-F5 angles. The Xe–F bonds of $F_6Xe(NCCH_3)_2$ can be classified into three groups: two equatorial F atoms adjacent to the presumed location of the Xe VELP [Xe1−F1: 1.981(2) Å; Xe1−F2: 1.9876(13) Å], two axial F atoms [Xe1−F3 and Xe1−F3A: 1.8936(11) Å], and two equatorial F atoms opposite to the Xe VELP [Xe1−F4: 1.868(2) Å; Xe1−F5: 1.873(2) Å]. The geometry of the XeF_6 moiety may be viewed as a C_{2v}-distorted AX_6E VSEPR arrangement (**5**) of the Xe VELP and six Xe−F bond pair domains, where the Xe VELP occupies a position between F1 and F2 in the equatorial Xe1–F1/F2–F4/F5 plane, causing the axial F3/F3A atoms to bend away from the equatorial VELP position towards F4/F5, resulting in an F3-Xe1-F3A angle of 156.90(7)°. When the Xe−N bonds (2.785(2) Å) are included in the description of the Xe coordination sphere, the F3/F3A, N1/N1A, and Xe1 atoms are seen to be coplanar within ±0.110 Å, with the Xe−N bonds avoiding the Xe VELP position.

The Raman spectra of **1** and **2**·CH_3CN are shown in Figure 3. Selected experimental and calculated gas-phase (PBE1PBE/aug-cc-pVTZ(-PP)) frequencies and assignments are listed in Table 1 and Table 2. Full lists, including the frequencies and assignments for coordinated CH_3CN, are provided in Tables S3 and S4, along with a detailed discussion. The frequency trends are well reproduced by the calculations. Factor-group analyses were performed to account for splittings that occur on some bands (Tables S5 and S6).

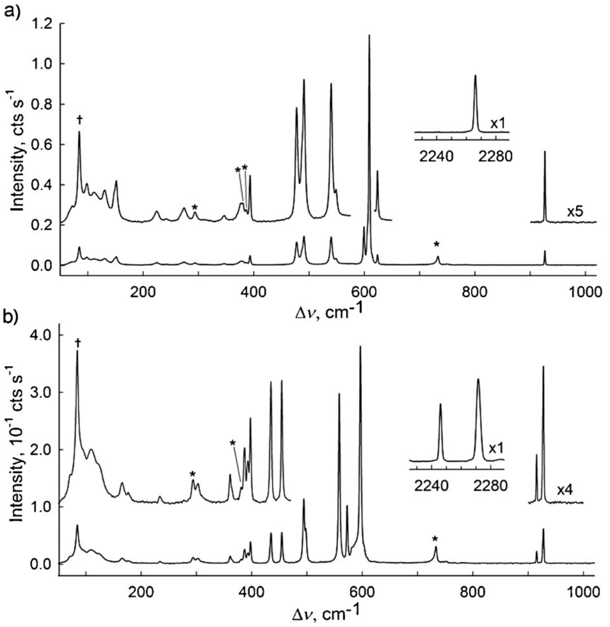

Figure 3. Raman spectra of a) **1** and b) **2**·CH_3CN recorded at −150 °C using 1064 nm excitation. Symbols denote FEP sample tube lines (*) and an instrumental artifact (†).

Table 1: Selected experimental and calculated Raman frequencies (cm^{-1}) and assignments for $F_6XeNCCH_3$.[a]

Exp.[b]	Calculated[c]	Assignment
624.1(4) 609.1(100)	632.5(75)[184]	A_1, $\nu_s(XeF_{3b})$
605.7 sh 599.5(13)	620.0(8)[211]	E, $\nu_{as}(XeF_{3a}) + \nu_{as}(XeF_{3b})$
548.4(1) 540.2(11)	557.5(18)[78]	A_1, $\nu_s(XeF_{3a})$
491.0(12) 477.5(9)	504.5(14)[110]	E, $\nu_{as}(XeF_{3a}) - \nu_{as}(XeF_{3b})$
345.9(1)	335.3(1)[10] 334.2(1)[1]	A_1, $\delta_s(XeF_{3b})$ E, $\delta_{as}(XeF_{3a}) + \delta_{as}(XeF_{3b})$
273.5(1)	246.8(1)[<1]	E, $\rho_r(XeF_{3a}) + \rho_r(XeF_{3b})$
223.9(1)	205.9(2)[17]	A_1, $\delta_s(XeF_{3a})$
150.6(3) 147.2(<1)	149.2(<1)[1]	E, $[\delta_{as}(XeF_{3a}) - \delta_{as}(XeF_{3b})] + \delta(XeNC)$
129.4(1)	106.1(1)[9]	A_1, $\nu(XeN)$

[a] See Table S3 for a full list of frequencies and assignments for all bands; abbreviations are given in the footnotes. [b] Values in parentheses denote relative Raman intensities. [c] PBE1PBE/aug-cc-pVTZ(-PP). Values in parentheses denote Raman intensities (Å amu^{-1}). Values in square brackets denote infrared intensities (km mol^{-1}).

In both adducts, high-frequency shifts occur for ν(CN), ν(CC), and δ(NCC), which is in accordance with the weak Xe−N bonding interaction that is indicated by the crystal structures and quantum-chemical calculations. The Xe−F stretches (**1**: 478–624 cm^{-1}; **2**·CH_3CN: 454–597 cm^{-1}) occur in ranges similar to those reported for gas-phase and matrix-isolated XeF_6,[6–8] but are shifted to lower frequencies. Weak bands at 129 and 110 cm^{-1} in the Raman spectra of **1** and **2**·CH_3CN, respectively, were assigned to ν(XeN). The low frequencies of the coupled δ(XeNC) modes (147–205 cm^{-1}) are also consistent with weak Xe−N interactions and highly deformable Xe-N-C angles, and likely account for the nonlinearity of this angle in the crystal structures of **1** and **2**·CH_3CN.

Binding energies for the Xe−N interactions in **1** and **2** were determined at the MP2/aug-cc-pVTZ(-PP) level of theory [Eqs. (3)–(5)]. The energy for free XeF_6 was approximated from structure **3** (Table S7) and used because it was not possible to optimize **4** at the MP2 level of theory.[26] The energy differences between **3** and **4** are 0.79 (CCSD(T)/CBS)[12] and 7.53 kJ mol^{-1} (CCSD(T)-F12b).[13]

$$XeF_6 + CH_3CN \rightarrow F_6XeNCCH_3 \qquad -157.1\ \text{kJ mol}^{-1} \qquad (3)$$

$$F_6XeNCCH_3 + CH_3CN \rightarrow F_6Xe(NCCH_3)_2 \qquad -129.5\ \text{kJ mol}^{-1} \qquad (4)$$

$$XeF_6 + 2\,CH_3CN \rightarrow F_6Xe(NCCH_3)_2 \qquad -286.7\ \text{kJ mol}^{-1} \qquad (5)$$

In conclusion, the adducts **1** and **2**·CH_3CN have been synthesized and structurally characterized by X-ray crystallography and Raman and NMR spectroscopy. They represent the first examples of Xe^{VI}−N bonds, and their structures provide structural evidence that is consistent with the stereochemical activities of their Xe VELPs. Both adducts are well isolated from one another in their crystal lattices, based on the long intermolecular contacts observed among their structural units, and provide the only examples of

Table 2: Selected experimental and calculated Raman frequencies (cm^{-1}) and assignments for $F_6Xe(NCCH_3)_2$.[a]

Exp.[b]	Calculated[c]	Assigment
596.6(100)	621.0(80)[161]	A_1, $\nu_s(XeF_{2c}) + \nu_s(XeF_{2b})_{small}$
581.1(sh)	604.9(6)[229]	B_1, $\nu_{as}(XeF_{2a}) + \nu_{as}(XeF_{2c})$
572.5(23)	598.7(6)[313]	B_2, $\nu_{as}(XeF_{2b})$
558.5(78)	565.6(28)[24]	A_1, $\nu_s(XeF_{2a}) + \nu_s(XeF_{2b}) - \nu_s(XeF_{2c})$
497.7(sh) 494.4(29)	509.1(16)[55]	A_1, $\nu_s(XeF_{2a}) - \nu_s(XeF_{2b})$
454.3(13)	487.1(8)[136]	B_1, $\nu_{as}(XeF_{2a}) - \nu_{as}(XeF_{2c})$
435.1(13)	407.2(1)[11]	A_1, $\delta(XeF_{2c}) + (XeF_{2a})_{small}$
360.8(3)	335.9(<1)[3] 334.7(<1)[2]	B_2, $\rho_r(XeF_{2b}) + \rho_w(XeF_{2c})$ B_1, $\delta(F_aXeF_b) - \delta(F_{a'}XeF_{b'})$
303.4(2)	278.9(1)[0]	A_2, $\rho_t(XeF_{2b}) + \rho_t(XeF_{2c})$
293.3(<1)	260.3(<1)[17]	A_1, $\delta(XeF_{2b}) - [\delta(XeF_{2a})]_{small}$
233.0(1)	201.6(<1)[10]	A_1, $\delta(XeF_{2a}) + \delta(XeF_{2b}) -$ $[\rho(XeF_{2c}) + \delta(XeNC)_{A+B}\ ip]_{small}$
176.2(<1) 165.1(2)	150.1(<1)[3] 149.5(<0.1)[0] 144.4(<0.1)[2]	B_2, $\rho_r(XeF_{2b}) + (\delta(XeNC)_{A\text{-}B})_{ip}$ A_2, $\rho_t(XeF_{2a}) + \rho_t(XeF_{2c}) + (\delta(XeNC)_{A\text{-}B})_{oop}$ B_1, $\rho_r(XeF_{2a}) + \rho_r(XeF_{2c}) + (\delta(XeNC)_{A+B})_{oop}$
109.6(1)	83.4(1)[<1] 76.6(<1)[6]	B_2, $\rho_w(XeF_{2a}) + (\delta(XeNC)_{A\text{-}B})_{ip}$ A_1, $\nu(XeN)_{A+B}$

[a] See Table S4 for a full list of frequencies and assignments for all bands; abbreviations are given in the footnotes. [b] Values in parentheses denote relative Raman intensities. [c] See the footnotes of Table 1.

a neutral ligand coordinated to XeF_6. The CH_3CN molecules weakly interact with Xe, thus the geometries of the XeF_6 units in **1** and **2** provide excellent approximations of the gas-phase geometries of **4** and **5**. The C_{3v} geometry of ground-state XeF_6 (**4**) has been accurately calculated for the gas-phase molecule.[12] Interestingly, the experimental geometrical parameters of the XeF_6 moiety in **1** are in very good agreement with those of **4**. Computational investigations on the nature of the Xe^{VI}–N bonding in **1** and **2** and the localization of the Xe valence electron lone pair are currently in progress in our laboratory and will be reported in due course.

Experimental Section

Caution! The adducts $F_6XeNCCH_3$ and $F_6Xe(NCCH_3)_2{\cdot}CH_3CN$ are highly energetic materials that may detonate when mechanically or thermally shocked (see the Supporting Information).

Synthesis of **1**: Xenon hexafluoride (0.1796 g, 0.7322 mmol) was condensed under static vacuum at −196 °C into a FEP reaction tube (outer diameter: 0.25 inch) equipped with a Kel-F valve. Freon-114 (ca. 0.2 mL) was condensed onto the XeF_6 at −196 °C. Direct contact between neat CH_3CN and XeF_6 was avoided by condensing a stoichiometric amount of CH_3CN (0.0298 g, 0.7259 mmol) onto the reactor walls above the frozen Freon-114 and XeF_6 layers at −196 °C. The sample was warmed to −78 °C, and frozen CH_3CN was carefully leached off the walls of the reactor with Freon-114. In this way, CH_3CN was diluted in Freon-114 prior to coming into contact with XeF_6. Moreover, XeF_6 has a low solubility in Freon-114 at −78 °C. After most of the CH_3CN had dissolved, the sample was warmed to −40 °C and mixed for 10 min. Removal of Freon-114 by pumping at −78 °C resulted in a white powder corresponding to Freon-114 solvated $F_6XeNCCH_3$. Further pumping on the solvate at −78 °C resulted in removal of Freon-114, yielding a white powder corresponding to pure **1**.

Synthesis of **2**·CH_3CN: Using a procedure similar to that for **1**, XeF_6 (0.1787 g, 0.7286 mmol) and CH_3CN (0.0896 g, 2.183 mmol) were combined. Removal of Freon-114 by pumping at −78 °C resulted in a white powder corresponding to pure **2**·CH_3CN.

Acknowledgements

We thank the Natural Sciences and Engineering Research Council of Canada for support in the form of a Discovery Grant (G.J.S.) and the Ontario Ministry of Training, Colleges, and Universities for graduate scholarships (J.H.).

Keywords: fluorine chemistry · noble-gas chemistry · Raman spectroscopy · xenon fluorides · X-ray crystallography

How to cite: *Angew. Chem. Int. Ed.* **2015**, *54*, 14169–14173
Angew. Chem. **2015**, *127*, 14375–14379

---

[1] L. S. Bartell, R. M. Gavin, Jr., H. B. Thompson, C. L. Chernick, *J. Chem. Phys.* **1965**, *43*, 2547–2548.
[2] R. M. Gavin, Jr., L. S. Bartell, *J. Chem. Phys.* **1968**, *48*, 2460–2464.
[3] L. S. Bartell, R. M. Gavin, Jr., *J. Chem. Phys.* **1968**, *48*, 2466–2483.
[4] K. Hedberg, S. H. Peterson, R. R. Ryan, B. Weinstock, *J. Am. Chem. Soc.* **1967**, *89*, 6466–6469.
[5] W. Harshberger, R. K. Bofn, S. H. Bauer, *J. Am. Chem. Soc.* **1967**, *89*, 6466–6469.
[6] H. Kim, H. H. Claassen, E. Pearson, *Inorg. Chem.* **1968**, *7*, 616–617.
[7] E. L. Gasner, H. H. Claassen, *Inorg. Chem.* **1967**, *6*, 1937–1938.
[8] H. H. Claassen, G. L. Goodman, H. Kim, *J. Chem. Phys.* **1972**, *56*, 5042–5053.
[9] J. N. Cutler, G. M. Bancroft, J. D. Bozek, K. H. Tan, G. J. Schrobilgen, *J. Am. Chem. Soc.* **1991**, *113*, 9125–9131.
[10] J. S. Tse, D. J. Bristow, G. M. Bancroft, G. J. Schrobilgen, *Inorg. Chem.* **1983**, *22*, 2673–2677.
[11] R. J. Gillespie, I. Hargittai, *The VSEPR Model of Molecular Geometry*, Allyn and Bacon, Boston, MA, **1991**.
[12] K. A. Peterson, D. A. Dixon, H. Stoll, *J. Phys. Chem. A* **2012**, *116*, 9777–9782, and references therein.
[13] L. Cheng, J. Gauss, J. F. Stanton, *J. Chem. Phys.* **2015**, *142*, 1–7.
[14] S. Hoyer, T. Emmler, K. Seppelt, *J. Fluorine Chem.* **2006**, *127*, 1415–1422.
[15] A. Ellern, A. R. Mahjoub, K. Seppelt, *Angew. Chem. Int. Ed. Engl.* **1996**, *35*, 1123–1124; *Angew. Chem.* **1996**, *108*, 1198–1200.
[16] G. J. Schrobilgen, J. H. Holloway, P. Granger, C. Brevard, *Inorg. Chem.* **1978**, *17*, 980–987.
[17] K. Seppelt, N. Bartlett, *Z. Anorg. Allg. Chem.* **1977**, *436*, 122–126, and references therein.
[18] M. Gerken, P. Hazendonk, J. Nieboer, G. J. Schrobilgen, *J. Fluorine Chem.* **2004**, *125*, 1163–1168.
[19] G. L. Smith, G. J. Schrobilgen, *Inorg. Chem.* **2009**, *48*, 7714–7728, and references therein.

[20] K. Koppe, J. Haner, H. P. A. Mercier, H.-J. Frohn, G. J. Schrobilgen, *Inorg. Chem.* **2014**, *53*, 11640 – 11661.
[21] D. S. Brock, V. Bilir, H. P. A. Mercier, G. J. Schrobilgen, *J. Am. Chem. Soc.* **2007**, *129*, 3598 – 3611.
[22] K. Koppe, H.-J. Frohn, H. P. A. Mercier, G. J. Schrobilgen, *Inorg. Chem.* **2008**, *47*, 3205 – 3217.
[23] A. Bondi, *J. Phys. Chem.* **1964**, *68*, 441 – 451.
[24] B. E. Pointner, R. J. Suontamo, G. J. Schrobilgen, *Inorg. Chem.* **2006**, *45*, 1517 – 1534.
[25] G. J. Schrobilgen, N. LeBlond, D. A. Dixon, *Inorg. Chem.* **2000**, *39*, 2473 – 2487.
[26] M. Kaupp, C. van Wüllen, R. Franke, F. Schmitz, W. Kutzelnigg, *J. Am. Chem. Soc.* **1996**, *118*, 11939 – 11950.

Received: August 14, 2015